Chapter 3

HAp Nanofibers Grown with Crystalline Preferential Orientation and Its Influence in Mechanical Properties of Organic-Inorganic Composite Materials

Eric M. Rivera-Muñoz, Rodrigo Velázquez-Castillo, Susana Alonso-Sierra, J. Rafael Alanís-Gómez, Beatriz Millán-Malo, Lauro Bucio-Galindo, Rafael Huirache-Acuña, Alejandro Manzano-Ramírez, Rufino Nava and Miguel Apátiga-Castro

Additional information is available at the end of the chapter

http://dx.doi.org/10.5772/intechopen.71850

Abstract

There are several synthesis techniques to obtain hydroxyapatite (HAp). Some use surfactant agents, amino acids or halogen salts to control structural nucleation and crystal growth. In others, the use of hydrothermal process to carry out the reaction is effective for HAp synthesis. Microwave-assisted hydrothermal method (MAHM) has been successfully applied in the synthesis of HAp nanostructures, which present well-defined morphologies, high crystallinity and high purity. This is important because nano-HAp is attracting interest as a biomaterial for use in prosthetic applications due to its similarity in size, crystallinity and chemical composition with human hard tissue. In this chapter, developments in obtaining HAp nanofibers, with a crystal growth with preferential orientation, as well as morphology control achieved by using the MAHM is discussed. Also, the synthesized fibers were used to cast ceramics with controlled and interconnected porosity through the modified gelcasting process. Then, these HAp ceramics were impregnated with a water solution of gelatin in order to obtain an organic-inorganic composite material, similar to natural bone tissue. The maximum compressive strengths were determined and the composite materials showed mechanical properties that make them suitable to be used as bone tissue implants.

Keywords: bottom-up synthesis, HAp nanofibers, mechanical properties, microwave-assisted hydrothermal method, biomimetic material

1. Introduction

Hydroxyapatite (HAp) is an inorganic compound made of calcium phosphate and hydroxyl groups, with a stoichiometry of ($Ca_{10}(PO_4)_6(OH)_2$) and a hexagonal crystal structure. Natural HAp is the main mineral constituent of hard human tissues such bones and teeth, and it has the same crystal structure, but a stoichiometry slightly different from the synthetic one since some calcium ions can be exchanged by other metallic ions, such magnesium or sodium. The production of synthetic HAp has acquired a great significance in recent years due to its excellent properties of biocompatibility, bioactivity, osteoconductivity and osteoinductivity. Those properties are produced, in part, by its similarity in structure and chemical composition to those in the natural HAp [1]. Consequently, synthetic HAp has been widely applied in health-related fields as a replace, bone reconstructing or implant material in the restoration of damaged bones or teeth [2].

In spite of HAp is mainly useful as a biomaterial for implants in bone tissue, other interesting application have been developed in recent years. Some authors have explored the use of the HAp piezoelectric properties [3–5], some HAp-collagen composite materials have been studied to be applied in bone regeneration and osteogenesis using their piezoelectric properties [6, 7] or other composite materials based on HAp use this property to be used as a immunosensor material [8]. In addition, this HAp property was also studied to analyze its impact in the design and development of ferroelectric memories and micro-electro-mechanical systems, and consequently, some materials have been obtained for those applications [9]. Other interesting uses of HAp have been reported as catalysts [10–12], especially for the synthesis of organic compounds [13, 14], and some application in obtaining ecological biofuels [15, 16]. Additionally, the HAp has been used in water treatments [17–19] and for the environment remediation [20–22] to remove heavy metals. All these diverse applications have made the HAp a quite interesting material and the relevance of its synthesis and production methods are still increasing.

2. Different hydroxyapatite synthesis methods

Several synthesis methods have been proposed by many scientists in order to obtain HAp. The morphology, dimensions, crystalline quality and purity of the synthesized HAp have an impact on its properties, and the properties determine the final application of the HAp; for that reason, those structural characteristics often tried to control the synthesis process. **Table 1** summarizes the different HAp synthesis methods, their reaction times and the corresponding obtained morphology.

Sol-gel is one of the most used methods to obtain HAp. Here, the chemical substances, used as precursors, are dissolved in water (wet chemistry), and then this solution are blended with some monomer molecules to form a sol (colloid) at the beginning of the reaction, and posteriorly, the

Type of reaction	Reaction time	Reaction features	Reaction temperature	Obtained morphology
Sol-gel	24–120 h	A little energy available inside the reactor	25–45°C	Nanoparticles nanorods
Solid-state reaction	Several hours	Diffusion difficulties, calcination process required	25–1250°C	Nanoparticles
Conventional hydrothermal	Several minutes	Inhomogeneous temperature inside reactor	170°C	Nanoparticles, nanowires, nanofibers and nanoplates

Table 1. Different HAp synthesis methods and their corresponding outcome.

polymerization process continues until the formation of the gel. The chemical reaction takes place at room temperature, and therefore, there is little amount of energy for the reaction and, consequently, it takes several days [23–25], and the morphology mainly produce are particles.

An interesting example of wet chemical reaction is obtaining HAp from eggshells. The hen eggshells are made basically of calcium carbonate. In the synthesis to obtain HAp, the eggshells are cleaned and milled; posteriorly, the powder undergoes an initial thermal treatment at 450°C to eliminate organic residues and after that, the calcination of the powder is made to transform the calcium carbonate into calcium oxide. This calcium oxide could be hydrated to form calcium hydroxide, which is put in reaction with a solution of phosphoric acid to finally obtain the HAp [26]. In a variation of this reaction, the calcium oxide could be put in contact with a water solution of calcium phosphate in order to obtain the HAp [27].

Other authors have used the calcium oxide to obtain HAp through a solid-state reaction. The calcium oxide is mixed with phosphorus oxide and other additives; then, the mixture is sintered inside an oven at 1250°C, and the HAp is finally obtained [28]. In other solid-state method to produce HAp, diammonium phosphate, sodium bicarbonate and calcium nitrate are used as the main precursors of the synthesis. The reactants are mixed in the proportion to achieve the stoichiometric of HAp and milled. The mixture is aged at room temperature and posteriorly, this blend is washed, dried and calcined to produce HAp [29]. In several cases, where a solid-state method was used to obtain the HAp, the final product was mixed with other by-products.

Although the aforementioned synthesis methods are important for the HAp obtention, in most of the works where those procedures were used the authors did not report a control on the morphology, size, crystalline quality or structural parameters of the HAp aggregates, which made suppose that those structural features were difficult to regulate through those methods.

In other more innovative synthesis methods, the production of HAp involves the use of different chemical substances such surfactants, amino acids or halogen salts to control the nucleation and crystal growth. The last one has, as a consequence, the control on the final morphology of HAp assembly [30–33]. Additionally, some of those methods use a conventional

hydrothermal process (CHP) to carry out the synthesis reaction. In CHP, the precursors are dissolved in water and put inside an autoclave. The heat to perform the reaction comes from the outer side of the reactor walls, and produces a temperature gradient in the solution. Mechanical agitation can be suitable to help in the heat distribution, and thus, try to generate a homogeneous temperature in the whole reactor. The steam produced by water increases the pressure on the solution and therefore, the boiling point of water is increased and the solution can reach a higher temperature. This higher temperature in the reactor can increase the reaction rate. A measured supply of heat makes possible to have a control on the temperature of the reacting solution, and thus, also a control on the pressure. These reaction conditions make the crystallizing substances possible in a short time; additionally, the size and crystal quality can be controlled during the crystal growth.

The CHP has demonstrated to be effective for the HAp synthesis; the use of this method has been improved due to the relative low cost and simplicity to synthesize HAp in a large scale and with a high purity [34–37]. The CHP experienced an important development when a microwave oven was used for the synthesis reaction. The microwaves provide the energy required to carry out a chemical reaction. The emission of microwaves could be focused into the reactor to reduce the amount of energy used. Thus, the microwave-assisted hydrothermal method (MAHM) was developed. Currently, this method is applied in the crystal growth of multiple substances with an excellent control on their morphology, size and preferential crystal orientation. Several works have reported the use of MAHM in the synthesis of HAp nanostructures, which possess well-defined morphologies, high crystallinity and purity [38–44]. According to literature, the structures more often synthesized by this synthesis method are nanoparticles, nanorods and nanofibers.

3. The microwave-assisted hydrothermal method

In the MAHM, the electric field of microwaves interacts with the dipole moment of molecules to produce heat. When a molecule is irradiated with a microwave, its dipole moment tries to align with the electric field vector. In an electromagnetic wave, the electric field is oscillating, and the dipole moment vector always attempts to be aligned with it. During the aligning process, the molecules disperse energy in the form of heat, which is produced by intermolecular frictions, collisions and dielectric losses. If the dipole moment of the molecules in a sample has not enough time to align with the electric field or if their reorientation occurs in a short time, the sample is not warming up.

In a conventional microwave oven, the magnetron produces electromagnetic wave with a frequency of 2.45 GHz and the waves possess energy of 0.0016 eV, but the electric field spins 4.9×10^9 times in a second. The dipole moment in the molecules has enough time to align with the electric field, but they cannot oscillate with the same frequency. Therefore, phase differences between the electric field and the dipole moments are generated, and these phase

http://dx.doi.org/10.5772/intechopen.71850

differences cause energy dispersion, and the lost energy has the form of heat, which is generated by the intermolecular collisions, frictions and dielectric losses. The heat produced increases the temperature of the sample. The presence of ions could accelerate the heating process. In that way, the reacting mixture inside the reactor could be heated quite homogeneously in a microwave oven. A better heat distribution produces a quite similar temperature into the whole reactor, and this cause that the chemical reaction take place with a similar rate everywhere into the reactor; thus, the crystal growth is rather homogeneous and, consequently, the size and the crystalline quality in the obtained crystal can be controlled.

Some materials can reflect the microwaves, for example, metals, and they do not allow the wave pass. In other materials, the microwaves produce low dielectric losses and then, those materials such glass, Teflon and quartz are transparent and they permit the microwave to pass. In MAHM, the vessels (reactors) are made of transparent materials. The absorbing materials are dielectrics and they have great dielectric losses generated by the interactions of microwaves; therefore, they can be heated by microwaves.

In this work, a detailed description is made of how the microwave-assisted hydrothermal method was used to prepare several types of HAp morphologies, from particles until nanofibers with a preferential crystalline orientation in the [300]. Some of these nanostructures had a high crystallinity and good purity, which were a consequence of the synthesis method used. A careful control on the operation conditions in the microwave oven concerning pressure and temperature allowed obtaining controlled heating and cooling rates to produce the HAp. The suitable chemical composition in the reacting mixture, and posteriorly, the use of the glutamic acid (GA) as the substance to guide and control the crystal growth of HAp nanostructures, were the main factors to obtain the different morphologies in the HAp assemblies.

Posteriorly, the HAp nanofibers were selected to produce a ceramic with a controlled porosity through the modified gelcasting process (MGCP). Porosity is rather relevant for the HAp in its application as a bone tissue implant. Dimension of pores must be large enough to permit the flow of nutrients, substances and cells with the purpose of carry out the regeneration process in the damaged bone tissue.

Once the porous ceramic was made, an organic phase made of protein was added in order to obtain an inorganic-organic composite material. The chemical interaction between both phases produced synergic mechanical properties.

4. Synthesis of HAp with different morphologies through MAHM

The long experimental way to obtain different morphologies in the HAp began with the formulation of the reacting mixture to perform the synthesis reactions. The chemical substances chosen for the synthesis were calcium nitrate [$Ca(NO_3)_2{\cdot}4H_2O$] as the source of calcium, monobasic potassium phosphate [KH_2PO_4] as the source of phosphate groups and

potassium hydroxide [KOH] to supply the hydroxyl groups. These inorganic compounds were dissolved separately in 100 ml of distillated water to achieve the stoichiometry of HAp. After that, the solutions were mixed and a 400-ml new dissolution (reacting mixture) was made, which was put inside eight Teflon tubes (50 ml each). The tubes were placed inside the microwave oven. This reaction was numerated as "1" (**Table 2**), and took place within the microwave oven at 150°C at a pressure of 690 kPa, 100 W power was used for a reaction time of 90 min. When the reaction was over, the final product was washed with ethanol, filtered and dried at room temperature. The HAp synthesized was analyzed by X-ray diffraction (XRD) by powders to identify the crystalline phases present in the sample and the respective diffractogram is shown in **Figure 1**(**a**). The phase identification was done by comparison using the powder diffraction file (PDF) data bank provided by the International Center for Diffraction Data (ICDD), and only one crystalline phase was found, which correspond to HAp, with PDF #86-1199. The presence of a single crystalline phase indicates that the synthesis method is suitable to

Reaction	$Ca(NO_3)_2$	Glutamic acid	HAp crystalline features	Obtained morphology
1	CNC	0.0	Good purity and satisfactory crystalline quality	Nanoparticles
2	CNC	0.2 (CNC)	Better crystalline quality and defined morphology	Nanowires-nanofibers
3	CNC	0.9 (CNC)	Excellent crystalline quality and preferential crystalline orientation	Nanofibers
4	CNC	2 (CNC)	Remarkable preferential crystalline orientation and structural organization	Nanofiber closely packed in microfibers
5	CNC	2.5 (CNC)	Decrease in the preferential crystalline orientation and a multilayer structure	Nanoplates

Table 2. Different HAp morphologies obtained by MAHM.

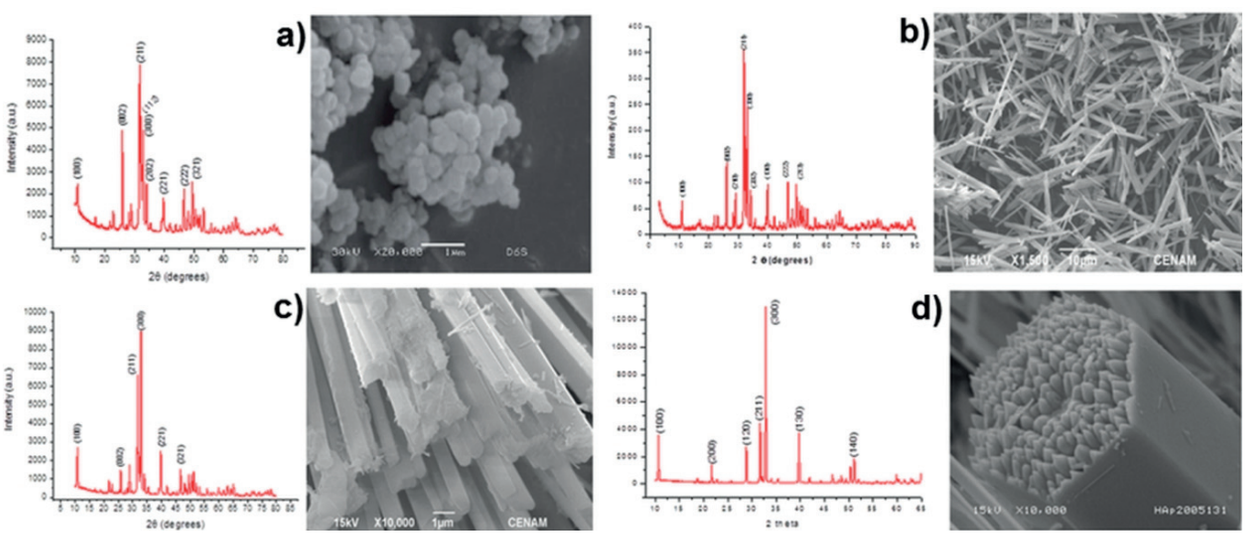

Figure 1. X-ray diffractograms and morphology of the HAp structures synthesized by the MAHM in reactions 1 (a), 2 (b), 3 (c) and 4 (d).

obtain HAp with a good purity. The diffractogram shows a background with a high noise level and the Bragg reflection are well-enough defined, those are indicative of an acceptable crystalline quality. Afterward, the HAp sample was observed by means of a scanning electron microscope, and the morphology found correspond to particles, as can be seen in **Figure 1**(**a**). The diameter in the particles was in the range from 90 until 160 nm. This reaction was useful to probe that HAp can be synthesized through the MAHM.

The next step was to include the glutamic acid (GA) in the chemical formulation of the reacting mixture and analyze the influence of this amino acid in the morphology of the HAp. The concentration of the other components in the reacting mixture was kept constant and the amount of GA varied. The reaction conditions in the microwave oven were the same as those described for reaction 1.

The GA has two carboxyl groups and one amine group. The nitrogen and the oxygen in these functional groups possess electron-pairs, which can be donated to the calcium ions in their empty "d" orbitals in order to form coordinate covalent bonds. Thus, the GA molecules bond the calcium ions and the acid can guide the crystal growth of HAp.

In reaction 2, the GA was added to the reacting mixture. The calcium nitrate concentration (CNC) was the reference and the GA concentration was 0.2 CNC in this reaction. The GA was dissolved in 200 ml of distilled water along with the calcium nitrate. At first, the solution was cloudy due to the GA solubility and for this reason, mechanical agitation was performed for about 2 h; posteriorly, the solution turned transparent and both chemical substances became dissolved. It is possible that the coordinate covalent bonds between Ca ions and the oxygen or nitrogen atoms could occur during this solution preparation, and consequently, the solubility of both substances was facilitated by these bonds formations.

The other reacting substances, KH_2PO_4 and KOH, were dissolved together in 200 ml of distilled water to form an additional solution. This solution was agitated for 15 min. Posteriorly, both dissolutions were mixed to produce 400 ml of the final reacting mixture, which is placed in eight Teflon vessels (50 ml each). These tubes are put inside the microwave oven, and the synthesis reaction was carried out using the same reaction conditions as reaction 1. Finally, the product was filtered and washed with distilled water.

X-ray diffraction analysis was performed to obtained the product, and again a single crystalline phase was obtained, and it was identified with the ICCD PDF #86-1199 (**Figure 1**(**b**)). The crystalline quality was improved in comparison to that showed by the HAp in reaction 1. Observation by SEM was also done to the sample, and an evident change in the morphology could be seen. This time the HAp possessed the morphology of nanowires as shown in **Figure 1**(**b**).

Reaction 3 was done with a GA concentration of 0.9 CNC. The reaction conditions were the same as those in reaction 1. The synthesized product from this reaction also showed a single crystalline phase identified as PDF #86-1199, but this time the Bragg reflection corresponding to the planes (300) at 32.92° in 2θ showed an increased intensity according to that reported in the mentioned PDF (as shown in **Figure 1**(**c**)). This is an evidence of a preferential crystalline orientation. The crystalline quality was increased again. The observation done by means of SEM revealed the morphology of well-defined fibers (**Figure 1c**).

For reaction 4, once again, the GA concentration was increased to 2 CNC, and the results were rather significant. This time, the X-ray diffraction showed a notorious increment in the intensity of the Bragg reflection produced by the (300) at 32.92°. This intensity is even higher than that for the (211), which is the most intense Bragg reflection according to the ICDD PDF #86-1199 (**Figure 1**(**d**)).

Similarly, the Bragg reflections produced by the planes (100) and (200) also experienced an increment in their intensities but in the diffractogram depicted in **Figure 1**(**d**), it is also possible to see a reduction in the intensity of the signal at 26°, which is generated by the (002). These changes in the Bragg reflection intensities are indicative of a remarkable preferential crystalline orientation on the HAp crystal structure.

Observations made using the SEM allowed seeing the morphology in the HAp obtained in this reaction, and the microscope revealed the morphology of microfibers as shown in **Figure 1**(**d**). This time, the microfibers were larger and thicker than those obtained in reaction 3, and they showed a quite smooth surface, their facets and ends looked well-defined, which is an evidence of a good-quality crystal growth. Additionally, all fibers showed a hexagonal cross section, their average diameter was 4.67 μm, and their lengths were in the range of hundreds of micrometers.

This morphology of fiber with a hexagonal profile allowed understanding the XRD results is depicted in **Figure 1**(**d**). During sample preparation for XRD experiments, most of the fibers laid on the sample holder and they acquired an arrangement in such way that their hexagonal profiles were perpendicular to the sample holder surface and their lengths were parallel to it (see **Figure 2**). As a result, most of the reciprocal vectors a* of the HAp crystal structure laid orthogonal to the surface and the possibilities to satisfy the diffraction conditions were increased. In contrast, a large number of reciprocal vectors c* laid parallel to the sample surface, and the probability to satisfy the Bragg conditions decreased considerably. Therefore, this fibers distribution made possible that the Bragg reflections produced by those planes orthogonal to the "a" axis in the HAp crystal structure (or "b" axis) had bigger intensity; In

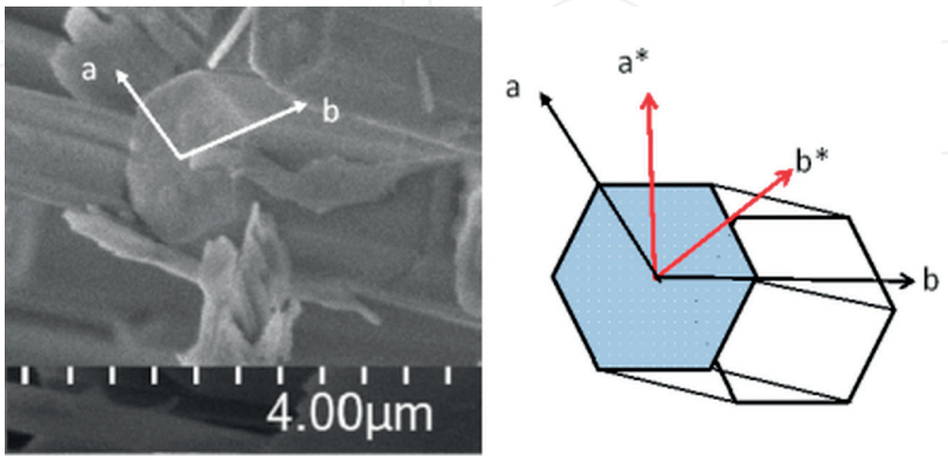

Figure 2. SEM micrograph showing the hexagonal profile in the HAp microfiber (left) and the schematic representation of the vectors "a" and "b" in the direct space, and the vectors "a*" and "b*" in the reciprocal space (right).

http://dx.doi.org/10.5772/intechopen.71850

contrast, the reflection generated by the planes perpendicular to the "c" axis decreased their intensity significantly in the X-ray diffraction experiments. Consequently, in the diffractogram shown in **Figure 1**(**d**), the contributions of the (300), (200) and (100) planes possess higher intensities and that corresponding to the (002) plane is nearly null.

In a closer observation on the hexagonal cross section of the fiber in **Figure 1**(**d**), it was possible to see the microfiber was formed of small fibers closely packed within its body. These small fibers possessed pointed-end structures as can be seen in **Figure 1**(**d**) and the right micrograph in **Figure 3**. Besides, some of the microfibers also had a pointed-end structure as it was depicted in the left image in **Figure 3**.

In the SEM micrograph on the right side of **Figure 3**, it is also possible to see a hole in the center of the microfiber profile, this empty space could be produced when some loose nanofibers slid out of the microfiber body, and then those free nanofibers were finally situated near of the microfiber. It is possible that the lone nanofiber indicated by the white arrow could have undergone a slide as described before.

Observation of nanofibers using high-resolution transmission electron microscopy (HRTEM) revealed that they had an average diameter of 97.5 nm, and a polycrystalline microstructure as can be seen in **Figure 4**(**b**) and (**c**). The average crystallite size was of 9.76 nm, which was calculated using the Digital Micrograph software.

Using that software, it was possible to obtain fast Fourier transforms (FFT) from the high-resolution images to analyze the crystal structure of the HAp in the nanofibers. The interplanar distances were also determined to identify the crystalline planes that contributed to form the images. In **Figure 5**, a bright field image of a nanofiber is depicted. In the upper right inset of **Figure 5**, a high-resolution micrograph of the nanofiber tip was showed. In this micrograph, it was possible to observe an arrangement of lines and dots, which were produced by the HAp crystal structure. The distances between lines were determined and the value of 0.344 nm

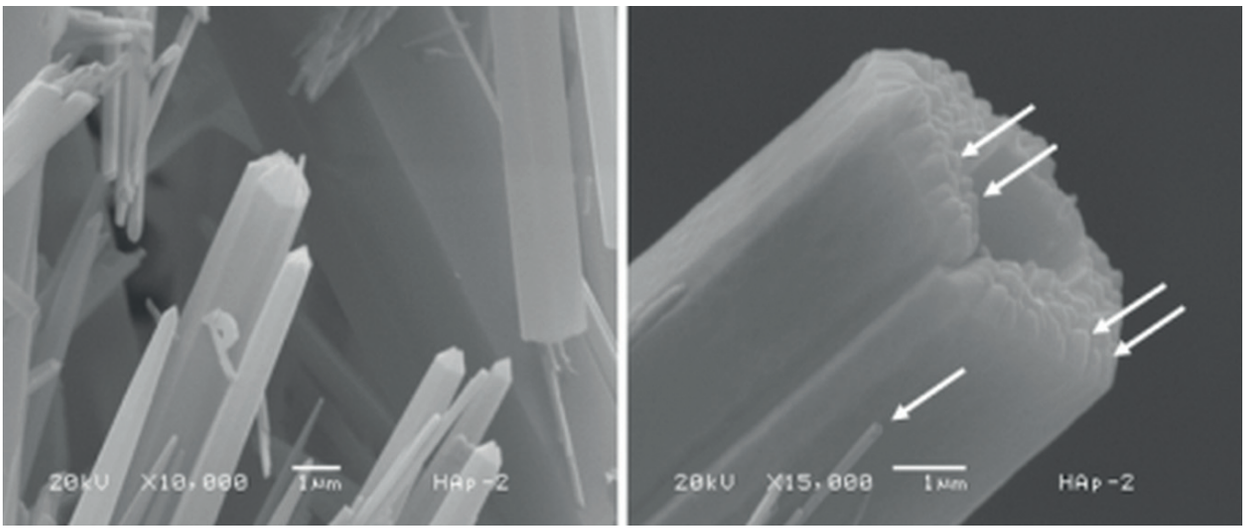

Figure 3. SEM micrographs of HAp microfibers showing the pointed-end (left) and how those nanofibers joint to form the microfiber structure (right), the white arrows indicate some nanofibers.

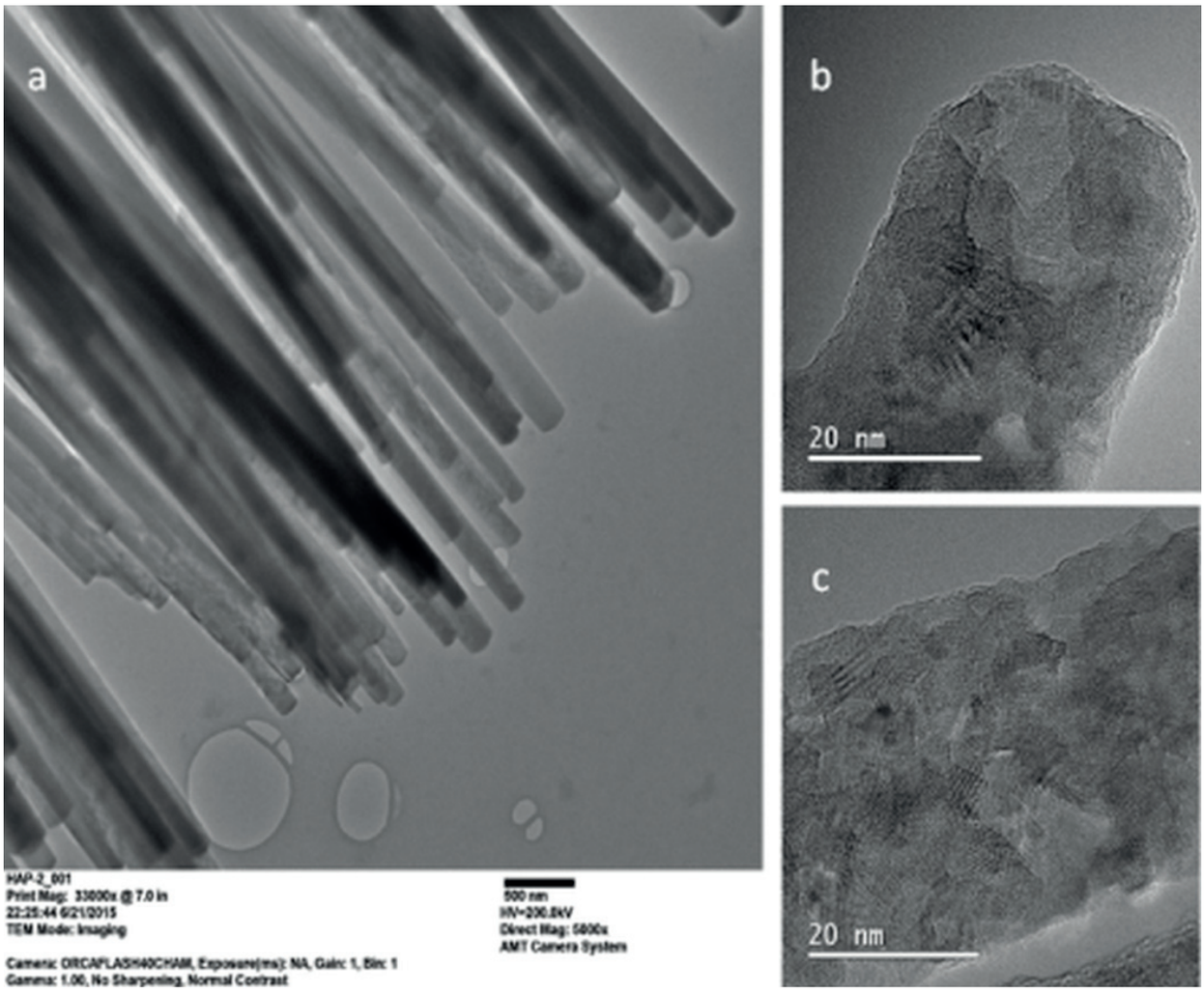

Figure 4. HRTEM images of nanofibers depicting their diameter size (a), and the polycrystallinity in their structure (b) and (c).

corresponds to the interplanar distance of (002) planes, and the distances between dots were of 0.295 nm, which were related to the (211) planes. A FFT was produced from the high-resolution micrograph and the dot pattern displayed in the bottom right inset was obtained.

The planes (002) generated the most intense dots in the pattern and this intensity is indicative of their abundance, which was also corroborated by the high-resolution micrograph in the upper inset of **Figure 5**. Other dots were produced by the planes (211). These crystalline planes are the most abundant according to the PDF 86-1199, but they are not numerous in the HAp obtained in this experiment. All dots in the FFT were laid on parallel lines and their arrangement is indicative of a high crystallinity. All (002) planes were stacked along the length of the nanofiber, and this stacking line was parallel to the "c" axis of the HAp crystal structure, this is indicative that the nanostructure was grown in the [002] direction as it was indicated in the upper right inset in **Figure 5**. These results were very significant because the preferred crystalline orientation found in the X-ray diffraction analysis, in the [300] direction, along with the SEM and HRTEM results indicates that the HAp fibers grow in [002] direction.

http://dx.doi.org/10.5772/intechopen.71850

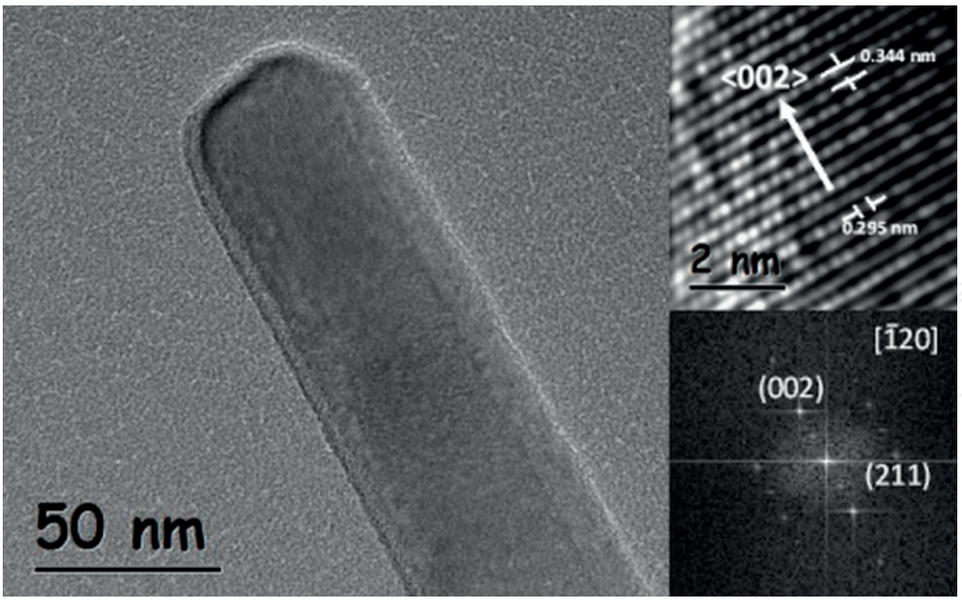

Figure 5. HRTEM image of a nanofiber showing its morphology. In the upper right inset, a high-resolution image of the fiber tip is displayed, the interplanar distances were calculated, and in the bottom right inset, a FFT was generated form the upper image and all dots were indexed.

These morphological and structural features of HAp fibers made them suitable to be used as the main material to elaborate porous ceramics, which must have porosity in the macro scale to allow the flow of nutrients and cells and consequently, a bone regeneration process could be possible.

Finally, once again the glutamic acid concentration increased in the reaction mixture and reaction 5 was performed to obtain another HAp structure. This time the concentration of glutamic acid was 250% related to the calcium nitrate content. The X-ray analysis of the product obtained in this reaction showed a small decrement on the intensity of the Bragg reflection corresponding to the (300) planes, and an increase in the intensity of the Bragg reflection at 26° related to the (002) planes, this is observed in the diffractogram in **Figure 6**(**a**). The latest is indicative that the preferential crystalline orientation is lesser in this product in comparison with the microfibers described before.

The HAp obtained in this reaction was observed by means of the SEM and the morphology of nanoplates was found. These nanoplates had different shape in the plane surface, and they had an average thickness of 62.3 nm. This morphology can be seen in **Figure 6**(**b**).

Similar to the case of the HAp microfibers, the nanoplates were formed by several small tickertapes or nanoribbons, which were joined to build the nanoplate surface (see **Figure 6**(**c**)). Besides, the thickness of these nanoplates were also formed by the stacking of those small nanoribbons in **Figure 6**(**c**) is possible to see some layers on the nanoplate surface and they were produce by the superposition of those nanoribbons. May be the whole nanoplate volume was formed by the union of several nanoribbons.

Possibly, during the crystal growth mechanism, the nanofibers or nanoribbons were formed, depending on the GA concentration in the reacting mixture, and their growing continued until

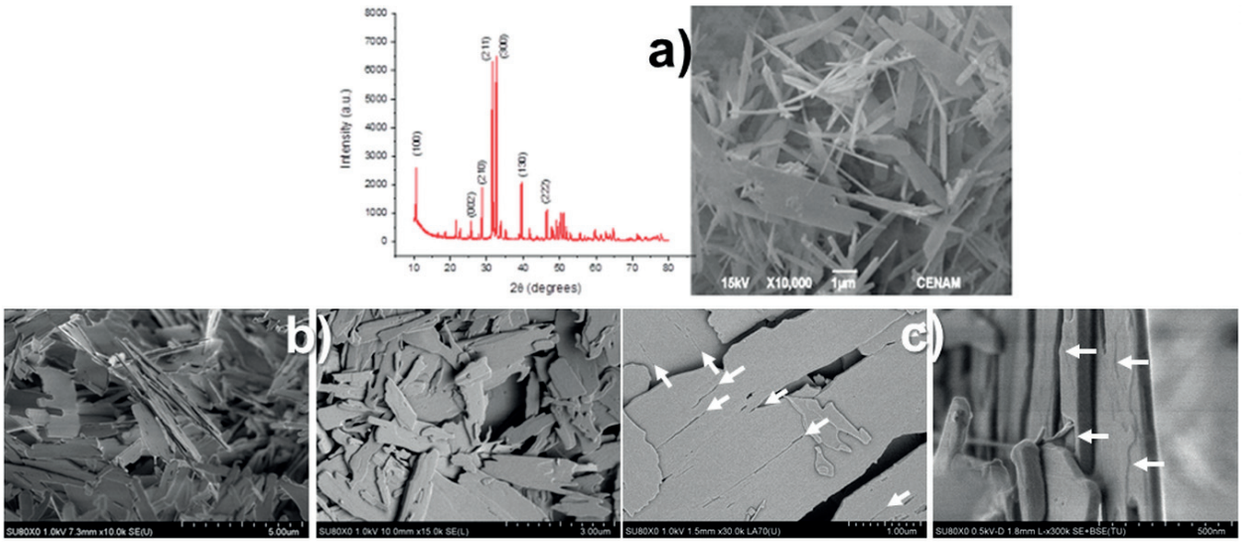

Figure 6. X-ray diffractogram of the HAp synthesized by the fifth chemical reaction and the morphology of nanoplates observed (a). SEM micrographs of nanoplates showing different shapes and sizes on the flat surfaces (b) and (c). The white arrows indicate the union between nanoribbons to form the flat surface, and the stacking of those nanoribbons to form the nanoplate thickness.

these nanostructures were linked to form the microfiber or nanoplate volume, respectively. The energy available within the reacting solution, especially in the regions close to the outer surface of the nanostructure, could be fused with the nanostructures to form a smooth surface. When the microfiber or nanoplate surface was degraded or corroded, it revealed that it was formed by the union of smaller pieces, corresponding to the nanofiber or nanoribbons.

5. Elaboration of HAp ceramics with interconnected porosity

Porosity plays a decisive role in the behavior of biomaterials. It is necessary to have sufficient pore size and interconnected porosity to promote osteoblasts to grow into a ceramic device [45, 46] and to allow cell penetration, internal tissue growth, vascular incursion and nutrient supply.

In order to manufacture HAp objects with different (and desired) shapes and sizes, which possess controlled and interconnected porosity, enough to permit cellular mobility and tissue ingrowth, it has used a successful process, named as modified gelcasting process (MGCP), previously reported by our group [47–50]. The key process is the proper use of a monomer-polymer blend, which can function as plasticizers, binders and dispersants and holds HAp powders or fibers together. During the polymerization, the slurry can be poured into silicone molds and a green body is obtained. PMMA micro balls (10–40 μm in diameter) were used as sacrificial porogens and oxalic acid was used to produce CO_2 bubbles during the polymerization to form the microporosity. Once the ceramic pieces are demolded, they are subjected to a thermal treatment in order to remove the polymers and promote a sintering of the HAp particles or fibers to obtain a ceramic with interconnected and controlled porosity. **Figure 7** shows HAp ceramic pieces with different shapes and sizes obtained through the MGCP.

http://dx.doi.org/10.5772/intechopen.71850

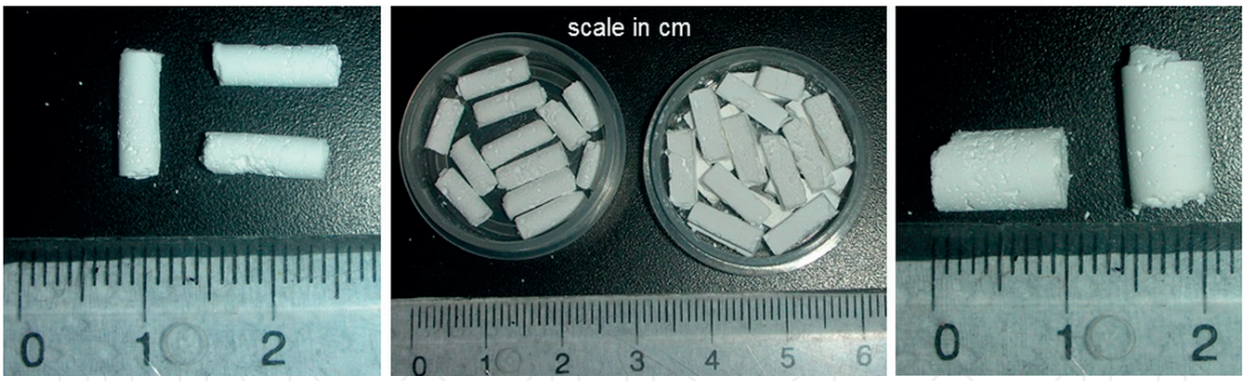

Figure 7. Hydroxyapatite objects molded in different sizes and shapes by the modified gelcasting process (scale in cm).

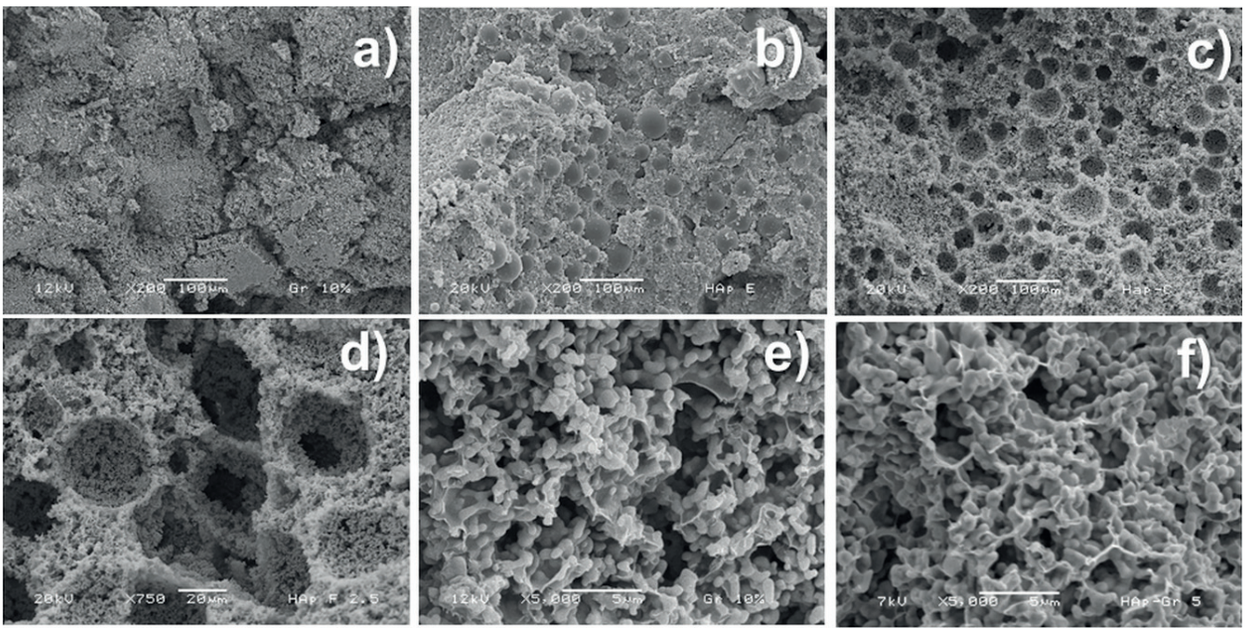

Figure 8. SEM micrographs of samples after gelcasting without PMMA micro balls (a) and with PMMA micro balls (b). SEM micrographs of HAp scaffold after polymer removal showing interconnected micro and macro porosity (c) and (d), and typical SEM micrographs of the HAp-based biomimetic organic-inorganic, composite material. The organic phase wet and links the HAp inorganic structure (e) and (f).

Figure 8(**a**) and (**b**) shows SEM micrographs of two demolded samples after the gelcasting process, in which polymers have not been eliminated. The difference between these two samples consists in that in the one of **Figure 8**(**a**) there is no PMMA micro balls, meanwhile in the sample of **Figure 8**(**b**) they can be clearly observed occupying spherical spaces that will generate the larger (or macro) porosity in the final HAp ceramic.

After the thermal treatment, polymers were removed and HAp fibers (or particles) are sintered to form a ceramic with interconnected porosity in micro (1–5 μm) and macro (20–40 μm) scales. This is relevant for the application as bone replacement because the osteocyte cells have a size between 100 and 500 nm [51], while osteoclast cells have a size of about 10 μm [52], which means that there is sufficient space to move through the porous structure. **Figure 8**(**c**)

and (**d**) show SEM micrographs in two different magnifications in which the interconnected micro and macro porosity is observed.

6. Obtaining the HAp-based organic-inorganic composite material

Due to the fact that the combination of polymers and hydroxyapatite to fabricate bone substitutes is a natural strategy, in order to elaborate a HAp-based organic-inorganic composite material, a water solution of gelatin (or collagen) was used as organic phase. HAp ceramics with interconnected and controlled porosity, obtained as described earlier, were used as inorganic phase and the final composite material was obtained by following the steps described in **Figure 9**.

Different water solutions of gelatin with 1.5, 2.5, 5, 6.75 and 7.5 wt%, were dripped to ceramic scaffolds to generate an organic-inorganic composite material. SEM analyzed the incorporation of gelatin (collagen) to the matrix and a typical example is shown in **Figure 8**(**e**) and (**f**). It is interesting to notice that the organic phase wet and links the HAp inorganic structure to form the organic-inorganic composite material in a similar way as in the natural bone tissue.

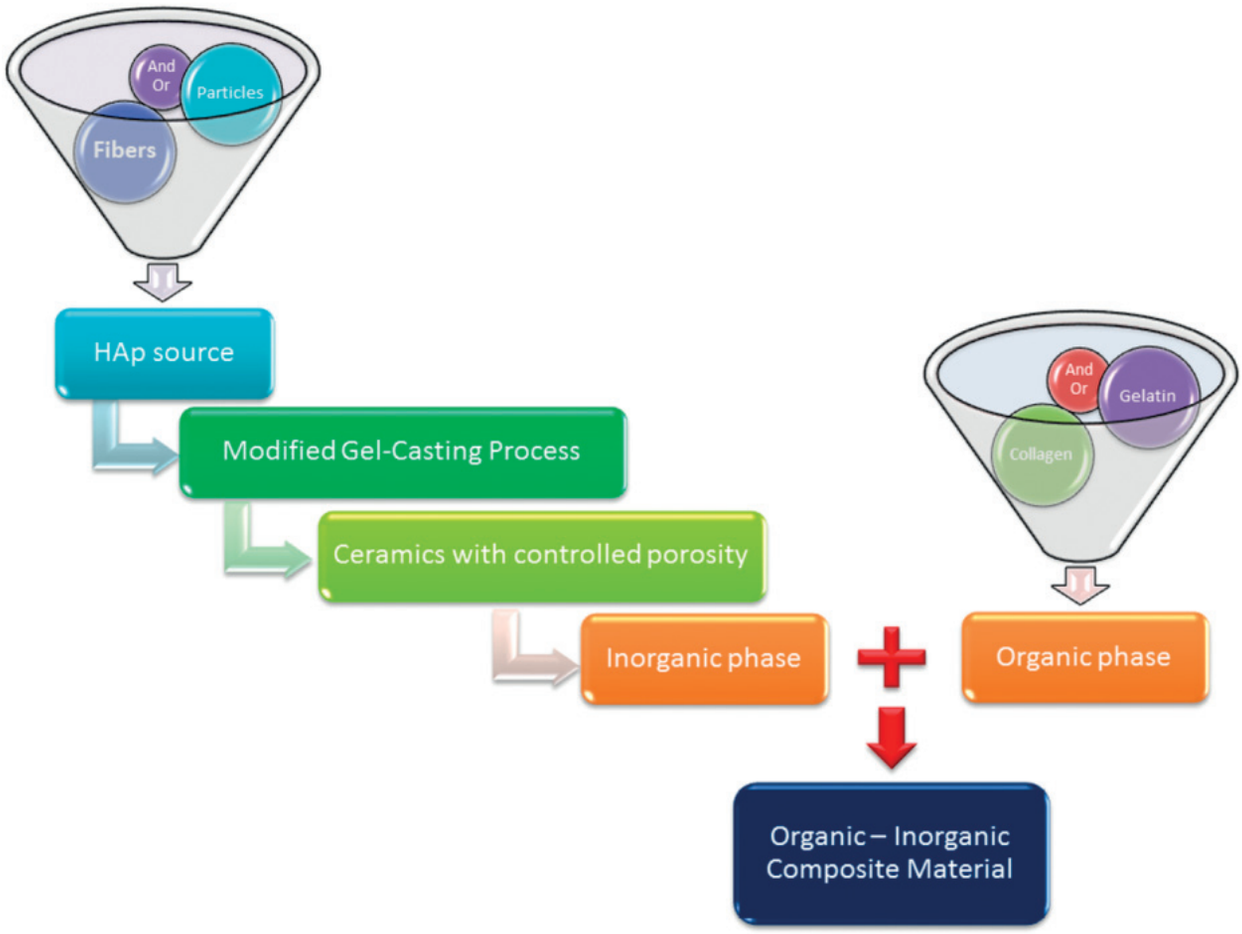

Figure 9. General procedure to obtain HAp-based organic-inorganic composite material.

http://dx.doi.org/10.5772/intechopen.71850

It has been established that a complex between calcium ions (Ca^{2+}) in HAp and —COO— groups in the amino acids in the organic phase is formed, which means that a chemical interaction between the organic and inorganic phases occurs to form the composite material [49, 50]. These interactions will play an important role in improving the mechanical properties of the final material.

Mechanical properties were evaluated under compression. **Figure 10**(**a**) shows a typical mechanical behavior of composite samples which corresponds to a typical non-linear elastic behavior showed by cellular materials and which agrees completely with the observations of SEM images as shown in **Figure 8**(**c**) and (**d**). The mechanical behavior shows two stages; in each of them, a linear behavior, corresponding to an elastic deformation is observed, after which a change in the slope of the curve is observed. At that point, the cells are deformed plastically until they reach the maximum compressive strength and begin to collapse, dissipating energy by breaking the bonds between the Ca^{2+} ions of the HAp and the —COO— groups of the organic phase mentioned above. Then, a densification of the material follows until the second stage is reached and the behavior is repeated until reaching a second maximum compressive strength (with a lower value). The highest of these maximum is reached due to the macroporosity while the following are reached due to the microporosity. Similar behavior has been described in different materials and studied by Maskery et al. [53].

The maximum compressive strengths were determined as a function of the gelatin concentration, as can be observed in **Figure 10**(**b**), and it is interesting to notice that there is a dramatic increase in the maximum compressive strength for the composite materials compared with the sample in which no organic phase was added (marked as WOP). Moreover, the maximum compressive strength increases as the amount of gelatin in the composite material increases, due to a synergic behavior between the inorganic and organic phases, to reach a value of 18 MPa for the sample with 7.5 wt% of gelatin. The aforementioned Ca—O bonds can absorb energy as sacrificial bonds, resulting in a synergic contribution to improve the mechanical properties of this composite material as well as due to the morphology of the HAp fibers. It is clear that for a hexagonal-shaped crystal, the direction in which it can withstand greater mechanical stresses is precisely [001] parallel to the axis of the hexagon. Consequently, the

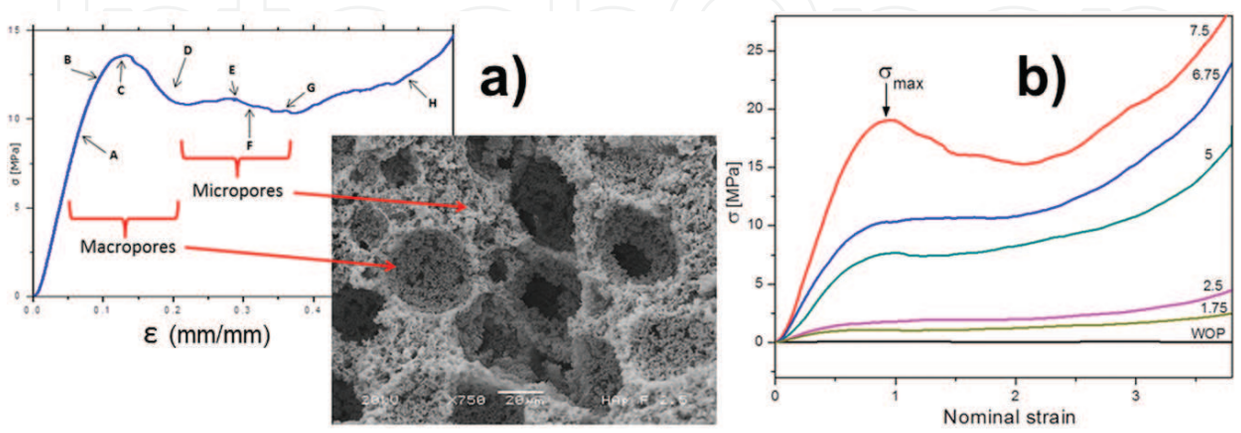

Figure 10. Mechanical compressive behavior of HAp-based biomimetic composite material (a). Stress-strain curves obtained in compressive tests for samples with different concentrations (wt%) of gelatin (b).

morphology of the HAp fibers obtained by the MAHM (grown with preferential orientation in the direction [001]), positively influences the improvement of the mechanical properties of the final HAp-based organic-inorganic composite material.

This value of 18 MPa, is 3.2 times higher than that reported for cancellous bone, and in the same order of magnitude for the cancellous-cortical bone tested under the same conditions [54], which implies that this biomimetic organic-inorganic composite material could be suitable for bone replacement.

7. Conclusions

After all experiments to synthesize different HAp nanostructures, it is possible to assure that the GA in the reacting mixture had a relevant impact on the final morphology of HAp clusters. This amino acid guided the HAp crystal growth and also leads the arrangement of small structures to form the final morphology, which was dependent on the GA concentration. In addition, this amino acid also allowed to obtain a preferential crystalline orientation in the [001] direction of the HAp crystal structure in most of the nanostructures obtained. The use of the MAHM made the synthesis of HAp with a high crystalline quality and purity easier.

Nanofiber was the most relevant morphology obtained in the synthesis reactions, and the arrangement of those to form microfibers with a hexagonal profile was unique. This morphology was selected to be used in the production of HAp porous ceramics due to its similarity with that of HAp morphology present in the human bone tissue.

The porous ceramic was successfully obtained through the MGP using the HAp microfibers. The micro and macro porosity were controlled in the ceramic body by the use of different polymers and chemical substances during the production process, and the pore size distribution was suitable to permit the flow of nutrients and cells.

The addition of protein to the porous ceramic allowed producing organic-inorganic composite materials in a biomimetic way. The strong chemical interaction between both phases leads to synergic mechanical properties in the composite materials.

Mechanical tests showed that the composite materials had a similar mechanical strength to that observed in the trabecular bone. These results suggest that this composite material can be an excellent option to be used as bone replacement or implant materials. In addition, the characterization of those composite materials proved that they also had an interconnected porosity in the micro and macro scales, which was proper to permit the natural regeneration processes of the human bone tissue.

Acknowledgements

Authors acknowledge the financial support of CONACYT scholarships and Fondo Salud 2013-01-201329. Authors also acknowledge Alicia del Real López and Carmen Peza Ledesma for

technical assistance in SEM analysis and Gilberto Mondragón Galicia and Jesús Arenas Alatorre for technical assistance in HRTEM studies.

Author details

Eric M. Rivera-Muñoz[1]*, Rodrigo Velázquez-Castillo[2], Susana Alonso-Sierra[2], J. Rafael Alanís-Gómez[2], Beatriz Millán-Malo[1], Lauro Bucio-Galindo[3], Rafael Huirache-Acuña[4], Alejandro Manzano-Ramírez[5], Rufino Nava[2] and Miguel Apátiga-Castro[1]

*Address all correspondence to: emrivera@fata.unam.mx

1 Center for Applied Physics and Advanced Technology, National Autonomous University of Mexico, Querétaro, Qro., México

2 Division of Research and Postgraduate, Faculty of Engineering, Autonomous University of Querétaro, Querétaro, Qro., México

3 Institute of Physics, National Autonomous University of Mexico, México, D.F., México

4 Chemical Engineering Faculty, Michoacan University of San Nicolás de Hidalgo, Ciudad Universitaria, Morelia, México

5 CINVESTAV-Querétaro, Libramiento Norponiente # 2000, Fraccionamiento Real de Juriquilla, Querétaro, México

References

[1] Campa J, Ulloa S, Bucio L, Belio IA, Velazquez R, Rivera E. Biomateriales: Fundamentos, técnicas y aplicaciones. 1st ed. Mexico: Universidad de Guadalajara; 2007. 127 p

[2] Avashnee C, Ilse W, Marei MK, Yasser EK, Moussa Rania M. Synthesis, properties, and applications of Please provide location name for the publisher in Ref. [2].hydroxyapatite. In: Gshalev Valeri S, Demirchan Aleksandra C, editors. Hydroxyapatite: Synthesis, Properties and Applications. Nova Sciences Publishers; 2012. pp. 91-132

[3] Silva CC, Pinheiro AG, Figueiró SD, Góes JC, Sasaki JM, Miranda MAR, Sombra ASB. Piezoelectric properties of collagen-nanocrystalline hydroxyapatite composites. Journal of Materials Science. 2002;**37**:2061-2070

[4] Bowen CR, Gitting J, Turner IG, Baxter F, Chaudhuri JB. Dielectric and piezoelectric properties of hydroxyapatite-$BaTiO_3$ composites. Applied Physic Letters. 2006;**89**(13):132906

[5] Bowen CR, Raman KVS, Topolov VY. Piezoelectric composites based on hydroxyapatie/barium titanate. Advances in Science and Technology. 2008;**54**:1-6

[6] Silva CC, Thomazini D, Pinheiro AG, Aranha N, Figueiro SD, Góes JC, Sombra ASB. Collagen-hydroxyapatite films: Piezoelectric properties. Materials Science & Engineering B. 2001;**86**(3):210-218

[7] Jianqing F, Huipin Y, Xingdong Z. Promotion of osteogenesis by a piezoelectric biological ceramic. Biomaterials. 1997;**18**(23):1531-1534

[8] Ding Y, Liu J, Wang H, Shen G, Yu RA. Piezoelectric immunosensor for the detection of a-fetoprotein using an interface of gold/hydroxyapatite hybrid nanomaterial. Biomaterials. 2007;**28**(12):21147-22154

[9] Damjanovic D. Ferroelectric, dielectric and piezoelectric properties of ferroelectric thin films and ceramics. Reports on Progress in Physics. 1998;**61**(9):1267-1272

[10] Tsuchida T, Yoshioka T, Sakuma S, Takeguchi T, Ueda W. Synthesis of biogasoline from ethanol over hydroxyapatite catalyst. Industrial & Engineering Chemistry Research. 2008;**47**(5):1443-1452

[11] Xu J, White T, Li P, He C, Han YF. Hydroxyapatite foam as a catalyst for formaldehyde combustion at room temperature. Journal of the American Chemical Society. 2010;**132**(38): 13172-13173

[12] Tsuchida T, Kubo J, Yoshioka T, Sakuma S, Takegushi T, Ueda W. Reaction of ethanol over hydroxyapatite affected by Ca/P ratio of catalyst. Journal of Catalysis. 2008;**259**(2): 183-189

[13] Sebti S, Tahir R, Nazih R, Boulaajaj S. Comparison of different lewis acid supported on hydroxyapatite as new catalysts of Friedel-craft alkylation. Applied Catalysis A: General. 2001;**218**(1–2):25-30

[14] Ogo S, Onda A, Yanagisawa K. Selective synthesis of 1-butanol from etanol over strontium phosphate hydroxyapatite catalysts. Applied Catalysis A: General. 2011;**402**(1–2): 188-195

[15] Chackraborty R, Bepar Si, Banerjee A. Application of calcined waste fish (Labeo rohita) scale as low-cost heterogeneous catalyst for biodiesel synthesis. Bioresource Technology. 2011;**102**(3):3610-3618

[16] Ngamcharussrivichai C, Nunthasanti P, Tanachai S, Bunyakiat K. Biodiesel production through transesterification over natural calciums. Fuel Processing Technology. 2010;**91** (11):1409-1415

[17] Jiang S-D, Yao Q-Z, Zhou G-T, Sheng-Quan F. Fabrication of hydroxyapatite hierarchical hollow microspheres and potential application in water treatment. Journal of Physical Chemistry. 2012;**116**(7):4484-4492

[18] Ozawa M, Hattori M, Satake K. Waste management and application of fish bone hydroxyapatite for waste water treatment. In: Proceedings of the International Symposium on Ecotopia Science 2007; November 23–25, 2007; Nagoya, Japan. Nagoya University; 2007. p. 957-958

[19] Wang F, Guo Y, Wang H, Yang L, Wang K, Ma X, Yao W, Zhang H. Facile preparation of hydroxyapatite with a three dimensional architecture and potential application in water treatment. CrystEngComm. 2011;**13**:5634-5637

[20] Boissona J, Ruttensb A, Mencha M, Vangronsveldb J. Evaluation of hydroxyapatite as a metal immobilizing soil additive for the remediation of polluted soils. Part 1. Influence of hydroxyapatite on metal exchangeability in soil, plant growth and plant metal accumulation. Environmental Pollution. 1999;**104**(2):225-233

[21] Seaman JC, Arey JS, Bertsch PM. Immobilization of nickel and other metals in contaminated sediments by hydroxyapatite addition. Journal of Environmental Quality. 2000;**30**(2): 460-469

[22] Jang SH, Jeong YG, Min BG, Lyoo WS, Lee SC. Preparation and lead ion removal property of hydroxyapatite/polyacrylamide composite hydrogels. Journal of Hazardous Materials. 2008;**159**(2–3):294-299

[23] Liu DM, Troczynski T, Tseng WJ. Water-based sol-gel synthesis of hydroxyapatite: Process development. Biomaterials. 2001;**22**(13):1721-1730

[24] Padmanabhan SK, Balakrishnan A, Chu M, Lee YJ, Kim TN, Cho SJ. Sol-gel symthesis and characterization of hydroxyapatite nanorod. Particuology. 2009;**7**(6):466-470

[25] Liu DM, Yang Q, Troczynski T, Tseng WJ. Structural evolution of sol gel derived hydroxyapatite. Biomaterials. 2002;**23**(7):1679-1687

[26] Baba AA, Oduwole IT, Salami FO, Adekola FA, Adeboye SE. Symthesis of hydroxyapatite from waste egg-shell by precipitation method. Ife Journal of Science. 2013;**15**(3):435-443

[27] Rivera E, Araiza M, Brostow W, Castaño V, Díaz JR, Hernández R, Rodríguez R. Synthesis of hydroxyapatite from eggshells. Materials Letters. 1999;**41**(3):128-135

[28] Pramanik S, Agarwal AK, Rai KN, Garg A. Development of high strength hydroxyapatite by solid-state-sintering process. Ceramics International. 2007;**33**(3):419-426

[29] Guo X, Yan H, Zhao S, Li Z, Li Y, Liang X. Effect of calcining temperature on particle size of hydroxyapatite synthesized by solid-state reaction at room temperature. Advanced Powder Technology. 2013;**24**(6):1034-1038

[30] Yan L, Li Y, Deng ZX, Zhuang J, Sun X. Surfactant assisted hydrothermal synthesis of hydroxyapatite nanorods. International Journal of Inorganic Materials. 2001;**3**(7):633-637

[31] Wang Y, Chen J, Wei k, Zhang S, Wang X. Surfactant-assisted synthesis of hydroxyapatite particles. Materials Letters. 2006;**60**(27):3227-3231

[32] Goudarzi A., Solati-Hashjin M., Moztarzadeh F. Surfactant assisted synthesis of hydroxyapatite nano-rods by aqueous precipitation and hydrothermal post-treatment. In: Jürgen G. Heinrich, editor. Proceedings of the 10th ECerS Conference; June 17–21, 2007; Berlin, Germany. Baden-Baden Göller; 2008. p. 964-968

[33] Zhang HG, Zhu Q, Wang Y. Morphologically controlled synthesis of hydroxyapatite with partial substitution of fluorine. Chemistry of Materials. 2005;**17**:5824-5830

[34] Liu HS, Chin TS, Lai LS, Chiu SY, Chung KH, Chang CS, Lui MT. Hydroxyapatite synthesized by a simplified hydrothermal method. Ceramamics International. 1997;**23**:19-25

[35] Liu J, Ye X, Wang H, Zhu M, Wang B, Yan H. The influence of pH and temperature on the morphology of hydroxyapatite synthesized by hydrothermal method. Ceramics International. 2003;**29**:629-633

[36] Hui P, Meena SL, Singh G, Agarawal RD, Prakash S. Synthesis of hydroxyapatite bioceramic powder by hydrothermal method. Journal of Mineral & Materials Characterization and Engineering. 2010;**9**(8):683-692

[37] Earl JS, Wood DJ, Milne SJ. Hydrothermal synthesis of hydroxyapatite. Journal of Physics: Conference Series. 2006;**26**:268-271

[38] Wang KW, Zhu YJ, Chen F, Cheng GF, Huang YH. Microwave-assisted synthesis of hydroxyapatite hollow microspheres in aqueous solution. Materials Letters. 2011;**65**(15–16): 2361-2363

[39] Qi C, Tang QL, Zhu YJ, Zhao XY, Chen F. Microwave-assisted hydrothermal rapid synthesis of hydroxyapatite nanowires using adenosine 5-triphosphate disodium salt as phosphorous source. Materials Letters. 2012;**85**:71-73

[40] Cao JM, Feng J, Deng SG, Chang X, Wang J, Liu JS, Lu P, Lu HX, Zheng MB, Zhang F. Microwave assisted solid-state synthesis of hydroxyapatite nanorods at room temperature. Journal of Materials Science. 2005;**40**(23):6311-6311

[41] Cabrera JL, Velázquez R, Rivera-Muñoz E. Synthesis of hydroxyapatite nanostructures using microwave heating. Journal of Nanoscience and Nanotechnology. 2011;**11**(6):5555-5561

[42] Meejo S, Maneeprakorn W, Winotai P. Phase and thermal stability of nanocrystalline hydroxyapatite prepared via microwave heating. Thermochimica Acta. 2006;**447**:115-120

[43] Kalita SJ, Verma S. Nanocrystalline hydroxyapatite bioceramic using microwave radiation: Synthesis and characterization. Materials Science and Engineering C. 2010;**30**:295-303

[44] Han JK, Song HY, Saito F, Lee BT. Synthesis of high purity nano-sized hydroxyapatite powder by microwave-hydrothermal method. Materials Chemistry and Physics. 2006;**99** (2–3):235-239

[45] Joschek S, Nies B, Krotz R, Göpferich A. Chemical and physicochemical characterization of porous hydroxyapatite ceramics made of natural bone. Biomaterials. 2000;**21**:1645-1658

[46] He L-H, Standard O, Huang T, Latella B, Swain M. Mechanical behavior of porous hydroxyapatite. Acta Biomaterialia. 2008;**4**:577-586

[47] Rivera-Muñoz E, Díaz J, Rodríguez R, Brostow W, Castaño V. Hydroxyapatite spheres with controlled porosity for eye ball prosthesis: Processing and characterization. Journal of Materials Science Materials in Medicine. 2001;**12**:305-311

[48] Rivera-Muñoz E, Velazquez R, Rodriguez R. Improvement in mechanical properties of hydroxyapatite objects with controlled porosity made by modified gelcasting process. Materials Science Forum. 2003;**426-432**:4489-4494

[49] Rivera-Muñoz EM, Velázquez R, Muñoz-Álvarez P. Mechanical characterization of hydroxyapatite-based, organic-inorganic composites. Materials Science Forum. 2007;**539-543**:583-588

[50] Alonso-Sierra S, Velázquez-Castillo R, Millán-Malo B, Nava R, Bucio L, Manzano-Ramírez A, Cid-Luna H, Rivera-Muñoz EM. Interconnected porosity analysis by 3D X-ray microtomography and mechanical behavior of biomimetic organic-inorganic composite materials. Materials Science and Engineering C. 2017;**80**:45-56

[51] Su BL, Sánchez C, Yang X-Y. Hierarchically Structured Porous Materials: From Nanoscience to Catalysis, Separation, Optics, Energy, and Life Science. Wiley-VCH Berlag GmbH & Co: Weinheim, Germany; 2011. 678 p

[52] Gough J, Notingher I, Hench L. Osteoblast attachment and mineralized nodule formation on rough and smooth 45S5 bioactive glass monoliths. Journal of Biomedcal Materials Research Part A. 2004;**68A**:640-650

[53] Maskery I, Aboulkhair N, Aremu A, Tuk C, Ashcroft I, Wildman R, Hague R. A mechanical property evaluation of graded density Al-Si10-Mg lattice structures manufactured by selective laser melting. Materials Science and Engineering A. 2016;**670**:264-274

[54] Ravaglioli K. Bioceramics. Materials, Properties and Applications. Great Britain: Chapman & Hall; 1992. 422 p

IntechOpen